Fossil Java Sea corals record Laurentide ice sheet disappearance

Thomas Mann[1,*], Tilo Schöne[2], Paul Kench[3], Kurt Lambeck[4], Erica Ashe[5], Dominik Kneer[6], Eddie Beetham[7], Julia Illigner[2], Alessio Rovere[8], Muh Aris Marfai[9], and Hildegard Westphal[1,10,11]

[1]Leibniz Centre for Tropical Marine Research (ZMT), 28359 Bremen, Germany
[2]Helmholtz-Zentrum Potsdam, Deutsches GeoForschungsZentrum GFZ, Telegrafenberg, 14473 Potsdam, Germany
[3]Department of Geography, National University of Singapore, 117568, Singapore
[4]The Australian National University, Research School of Earth Sciences, Canberra, ACT 0200, Australia
[5]Department of Earth and Planetary Sciences, Rutgers University, New Brunswick, New Jersey 08901, USA
[6]Alfred Wegener Institute for Polar and Marine Research, Wadden Sea Station Sylt, 25992 List, Germany
[7]Tonkin and Taylor International Ltd., Auckland 1010, New Zealand
[8]Department of Environmental Sciences, Informatics and Statistics, Università Ca' Foscari, 30172 Venice, Italy
[9]Geography Faculty, Gadjah Mada University, 55284 Yogyakarta, Indonesia
[10]Department of Geosciences, Universität Bremen, 28359 Bremen, Germany
[11]Physical Science and Engineering Division, King Abdullah University of Science and Technology (KAUST), Thuwal 23955-6900, Saudi Arabia

ABSTRACT

The Laurentide ice sheet was the largest late Pleistocene ice mass and the largest contributor to Holocene pre-industrial sea-level rise. While glaciological dates suggest final ice sheet melting between 8 and 6 ka, inversion of sea-level data indicates deglaciation at ca. 7 ka. Here, we present new chronostratigraphic constraints on Laurentide ice sheet disappearance based on Holocene relative sea-level observations from the tectonically stable north coast of Java, Indonesia. Age-elevation data from the flat upper surfaces of 13 fossil intertidal corals (i.e., microatolls) indicate that the Java Sea experienced a relative sea level of 1.3 ± 0.7 m above present between 6.9 and 5.3 ka. To determine uncaptured relative sea-level trends within the observational uncertainties of this apparently constant highstand, we analyzed the internal structure of three sliced microatolls from the same site to produce a high-resolution data set. These data were used to statistically model relative sea-level rates and trends. Employing the data with the model provided evidence for a short-lived rise of relative sea level from 1.0 ± 0.3 m above present at 6.7 ± 0.1 ka to 1.9 ± 0.3 m above present at 6.4 ± 0.1 ka. The end of this rise likely represents the last input of meltwater from the vast Laurentide ice sheet, which, consequently, collapsed at least 400 yr later than assumed by some widely used models of glacial isostatic adjustment. Incorporating these new results into such predictive models will help to better understand the geographical variability of future sea-level rise as a result of global warming.

INTRODUCTION

Outside regions of major tectonics, sea-level change during glacial cycles is driven by the mass exchange between grounded ice sheets and the oceans, and its associated planetary deformation. The isostatic signature of this mass exchange varies geographically, according to whether the ice or water load is dominant, and locally, according to rheological parameters that are depth-dependent and laterally variable (Mitrovica and Peltier, 1991; Lambeck, 1993; Lambeck and Chappell, 2001; Mitrovica and Milne, 2002; Woodroffe et al., 2012). Predictive models of past and ongoing isostatic responses are important to constrain key processes of future relative sea-level (RSL) rise due to global warming. Such models rely on information about the ice-sheet evolution and the planet's rheology.

Glaciological chronostratigraphic constraints provide information on the evolution of large ice masses such as the vast North American Laurentide ice sheet (LIS). Typically based on ^{14}C dating of organic material beneath glacial till deposits, LIS deglaciation was identified to have occurred between 8 and 6 ka (Dyke and Prest, 1987; Dyke et al., 2002). Glaciological constraints have been adopted, for example, by Peltier (2004), Peltier et al. (2015), and Lambeck et al. (2017) to reconstruct the deglaciation chronology in their isostatic models. Due to the unknown time that elapsed between deposition of the dated material and ice retreat, however, ^{14}C data provide minimum-limiting information only. Later studies circumvented this problem through cosmogenic [10]Be dates and constrained LIS melting to 7.1–6.3 ka (Carlson et al., 2008; Ullman et al., 2016).

Geological observations of past RSL change provide further information on ice dynamics to calibrate isostatic models. Importantly, the inversion of such evidence from regions distant to the former ice sheets (i.e., far field) provides data to quantify both the parameters of the ice-sheet evolution that are missing from the glaciological database and the rheological parameters that define the response to ice-water surface loading (Lambeck, 1993). In the global model of glacial isostatic adjustment applied in this work, inversion of far-field RSL data, and its associated uncertainties, was interpreted to indicate the end of significant Northern Hemisphere deglaciation at 6.8 ka (Lambeck et al., 2014).

This study presents a synthesis of RSL data inferred from mid-Holocene coral microatolls

Thomas Mann [ORCID] https://orcid.org/0000-0002-9182-2741
*Now at Bundesanstalt für Geowissenschaften und Rohstoffe (BGR), 30655 Hannover, Germany; thomas.mann@bgr.de.
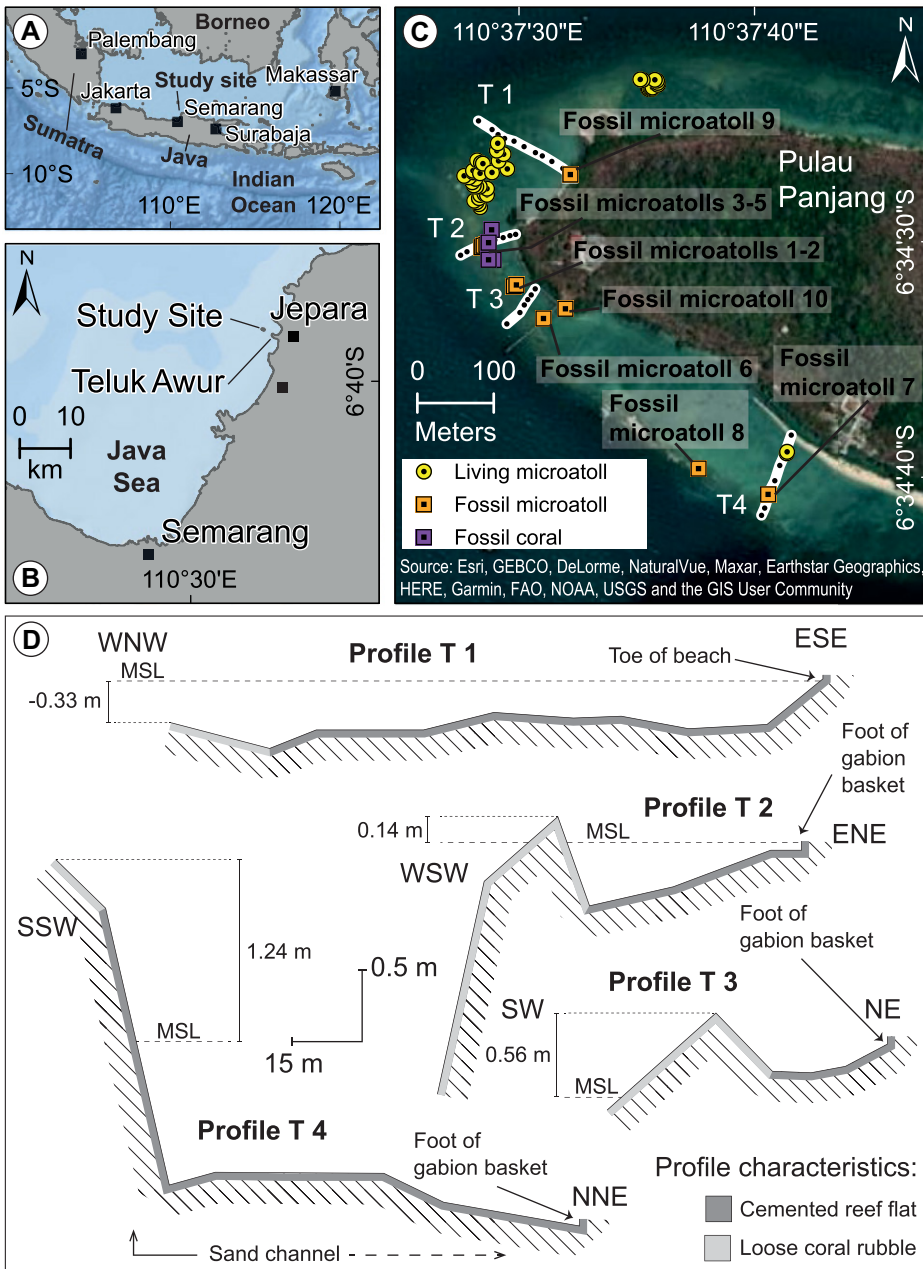
Figure 1. Geography and geomorphology of study site. (A) Overview map of broader study area (World Geodetic System 1984 projection). (B) Close-up map of study area and location of study island. (C) Satellite image of study island Pulau Panjang. Locations of relative sea-level (RSL) proxies and geomorphic transects (T1–T4) are indicated. (D) Reef flat geomorphology along four transect profiles T1–T4 (30× vertical exaggeration; MSL—mean sea level).

side the storm belt. Consequently, large corals interpreted as RSL indicators in this study have likely not been relocated by storm waves. Second, the Java Sea forms the southeastern margin of the tectonically stable Sunda Shelf. Jepara is located more than 400 km north of the Sunda megathrust, and so tectonic uplift is unlikely (Sobolev et al., 2007). Around the study site, only a few deep-seated earthquakes have been recorded, all of minor magnitude and without vertical displacement effects at the surface (Simons et al., 2007; see also Supplemental Material[1]). Third, only one previous RSL reconstruction exists nearby, at Teluk Awur (Azmy et al., 2010), and after data standardization, this record provides evidence of higher RSL (+~1.3 m) that remained constant (within the observational accuracies) between 6.7 and 5.3 ka (Mann et al., 2019).

METHODS

Our RSL reconstruction followed a standardized approach with verifiable age and elevation uncertainties (Shennan et al., 2015; Khan et al., 2019). We constrained mean sea level (MSL) at Pulau Panjang to 0.76 ± 0.12 m (2σ) above the World Geodetic System 1984 (WGS84) ellipsoid based on modern global navigation satellite system (GNSS) data, and we reduced our surveys to this datum. We surveyed two types of RSL coral proxies (Figs. 1 and 2): The first proxy was fossil microatolls (*Porites*, *Goniastrea*, and *Heliopora* spp.) with annular shapes and flat upper surfaces. Similar to previous studies, we treated the microatoll data as RSL index points that provide upper and lower boundaries (Woodroffe et al., 2012; Kench et al., 2020). The second proxy, fossil in situ corals without microatoll morphology, was interpreted as marine-limiting data indicating that RSL was higher during their growth (Yokoyama and Esat, 2015). The indicative range (IR) and reference water level (RWL) of each index point were determined based on geomorphic observations regarding the possibility of microatoll survival above open-water low-tide levels (i.e., ponding) and the vertical range of living specimens, largely around low tide levels (-0.74 to -0.21 m MSL, $n = 43$).

Elevations of RSL proxies (10 RSL index points, four marine-limiting data points) and the reef flat geomorphology were measured with differential GNSS. We applied an IR of 0.53 m and a RWL of -0.48 m for nonponded microatolls. For specimens where ponding during their lifetime could not be excluded, we applied a conservative IR of 1.65 m and RWL of -0.29 m, based on the vertical difference between modeled low-

Supplemental Material. Supplemental text and tables. Please visit https://doi.org/10.1130/GEOL.S.22687981 to access the supplemental material, and contact editing@geosociety.org with any questions.

---

at the tectonically stable north coast of Java, Indonesia. Upward growth of nonponded microatolls is constrained by low water levels, rendering their upper surfaces as precise indicators for RSL change (Scoffin and Stoddart, 1978; Smithers and Woodroffe, 2000). Our results provide new constraints with which to calibrate predictive models of isostatic response. Furthermore, results are of societal importance because instrumental and proxy records of RSL change are short in Indonesia, yet the impacts of future RSL rise on communities in this region will likely be profound.

STUDY SITE

Pulau Panjang is a sand cay on top of a coral reef platform in the marginal Java Sea 2 km offshore Jepara at the north coast of central Java, Indonesia (Fig. 1). The windward northwestern margin of the intertidal reef flat has a rubble sheet, and the vegetated island is located on the central platform. Living coral occurs along the windward reef margin. The tidal cycle is mixed semi-diurnal with a maximum tidal range of 1.4 m.

The Java Sea is a well-suited far-field region for RSL reconstructions: First, it is located out-

   www.gsapubs.org | Volume 51 | Number 7 | GEOLOGY | Geological Society of America

Downloaded from http://pubs.geoscienceworld.org/gsa/geology/article-pdf/51/7/631/5897138/g51038.1.pdf
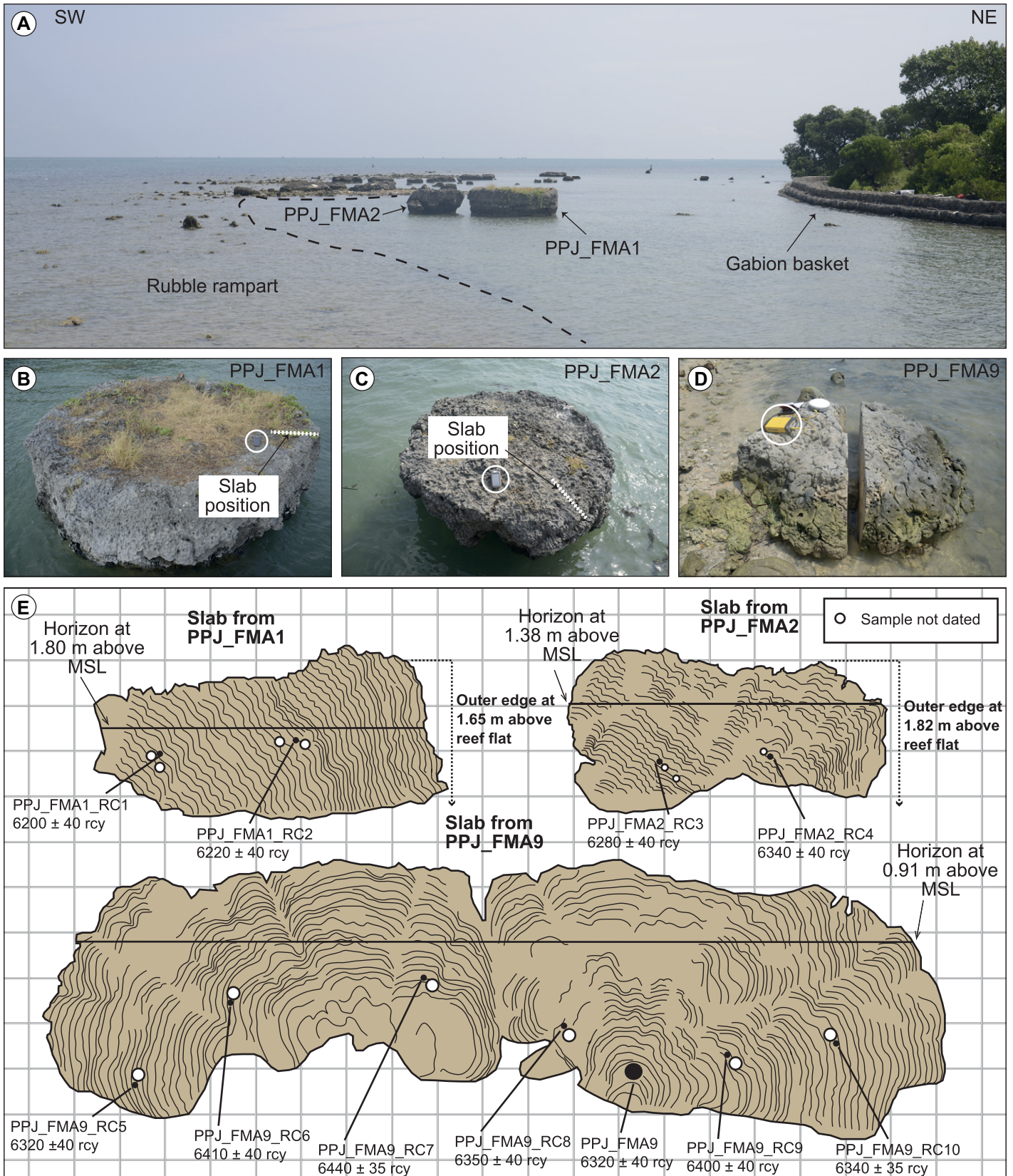by GeoForschungsZentrums Potsdam user

Figure 2. Microatolls on Pulau Panjang. (A) Field picture from western reef platform where numerous massive fossil microatolls are exposed. Height of upper gabion basket step is ~0.5 m. (B–D) Field photographs of three sliced microatolls. Global positioning system (GPS) units for scale (circled) are ~0.12 m (B, C) and 0.2 m (D). (E) Digitized images of X-rayed microatoll slices where growth increments are visible. Background raster has width of 0.1 × 0.1 m; MSL—mean sea level; rcy—radiocarbon yr B.P.

est astronomical tide and mean high water neaps (Egbert and Erofeeva, 2002). Three nonponded fossil microatolls with mostly pristine surface morphologies were slabbed using hand saws and X-rayed, and their internal structures were investigated as RSL proxy indicators following Meltzner and Woodroffe (2015).

Accelerator mass spectrometry radiocarbon ages were determined from aragonitic (X-ray diffraction >93% aragonite) samples. Conventional radiocarbon ages were calibrated to thousands of years B.P. (ka) with OxCal (Ramsey, 2008) using the marine calibration data set Marine20 (Heaton et al., 2020) and a Delta-R value of -64 ± 70 ^{14}C yr (Southon et al., 2002). Weighted averages of ^{14}C dates from subsamples of microatoll slab growth bands were determined using the D(·) function in OxCal.

We employed a hierarchical statistical model to the RSL proxy indicator data wherein the timing was analyzed through floating chronologies (Ashe et al., 2019).

The glacial rebound solutions used here were developed at the Australian National University (ANU; Nakada and Lambeck, 1988; Lambeck, 1993; Lambeck et al., 2014, 2017). The applied isostatic model focuses on regional solutions for both the rheology and load parameters following an iterative process where resulting viscosity parameters become effective parameters that reflect the response of different parts of the mantle and that are not directly comparable. For this study, we used a three-layer far-field continental margin Earth model based on inversions of a global suite of far-field RSL data reaching back to marine isotope stage 5 (Lambeck et al.,

2014). Resulting viscosity parameters suggested an effective elastic lithospheric thickness that ranged between 45 and 80 km, an upper-mantle viscosity that is well constrained to (1.5–2.5) $\times$ 10^{20} Pa·s, and a lower-mantle viscosity for which the upper limit is rather loosely constrained to (1.7 to >20) $\times$ 10^{22} Pa·s. Full details are available in the Supplemental Material.

RESULTS

Upper surfaces of fossil microatolls occupy an elevation range between 0.46 and 1.49 m MSL, whereas fossil corals (marine limiting) have lower elevations from -0.08 to 0.59 m MSL (Table 1). Dated samples provided calibrated age ranges between 6.9 and 6.3 ka. The two oldest, potentially ponded microatolls (PPJ_FMA7 and PPJ_FMA8) are located in a

TABLE 1. SUMMARY INFORMATION ON AGES AND ELEVATIONS OF RELATIVE SEA-LEVEL (RSL) PROXIES APPLIED

Sample name	Lab. no.	Radiocarbon age (^{14}C yr B.P. $\pm 1\sigma$)	Calibrated 2σ age range (calendar yr B.P.)	Modelled 2σ age range (calendar yr B.P.)	Elevation 2σ range (m MSL)	Indicative meaning	Indicative range (m)	Reference water level (m MSL)	RSL 2σ envelope (m MSL)
Fossil microatolls (RSL index points)									
PPJ_FMA3	Poz-83607	6310 ± 40	6730–6385	–	0.68–1.13	Vertical range of living microatolls	0.53	−0.48	1.04–1.73
PPJ_FMA4	Poz-83608	6330 ± 40	6744–6398	–	0.49–0.88	Vertical range of living microatolls	0.53	−0.48	0.83–1.49
PPJ_FMA5	Poz-83609	6340 ± 40	6758–6408	–	0.50–1.05	Vertical range of living microatolls	0.53	−0.48	0.87–1.64
PPJ_FMA6	Poz-83610	6250 ± 40	6654–6314	–	0.57–1.03	Vertical range of living microatolls	0.53	−0.48	0.93–1.63
PPJ_FMA7	Poz-83611	6490 ± 30	6934–6599	–	0.46–0.84	MHWN to LAT[†]	1.65	−0.29	0.09–1.78
PPJ_FMA8	Poz-83613	6500 ± 40	6953–6597	–	0.67–1.15	MHWN to LAT[†]	1.65	−0.29	0.34–2.05
PPJ_FMA10	Poz-83615	6410 ± 40	6848–6485	–	1.15–1.49	Vertical range of living microatolls	0.53	−0.48	1.48–2.11
TA H1-2 / SLCC149*	TA H1-2	5400 ± 80	5817–5341	–	0.09–1.11	Vertical range of living microatolls	0.53	−0.48	0.50–1.65
TA H1-5 / SLCC150*	TA H1-5	5720 ± 80	6173–5697	–	0.29–1.31	Vertical range of living microatolls	0.53	−0.48	0.70–1.85
TA H1-6 / SLCC151*	TA H1-6	6280 ± 80	6745–6295	–	0.19–1.21	Vertical range of living microatolls	0.53	−0.48	0.60–1.75
TA H2-1 / SLCC152*	TA H2-1	6120 ± 80	6597–6149	–	0.39–1.41	Vertical range of living microatolls	0.53	−0.48	0.80–1.95
TA H2-6 / SLCC153*	TA H2-6	5470 ± 80	5886–5451	–	0.49–1.51	Vertical range of living microatolls	0.53	−0.48	0.90–2.05
TA H2-7 / SLCC154*	TA H2-7	6010 ± 80	6451–5996	–	0.49–1.51	Vertical range of living microatolls	0.53	−0.48	0.90–2.05
Fossil microatoll slices (RSL proxy indicators)									
PPJ_FMA1	Poz-83603	6340 ± 40	6758–6408	6622–6412	–				
PPJ_FMA1_RC1	Poz-106802	6200 ± 40	6607–6279	6595–6385	–				
PPJ_FMA1_RC2	Poz-106803	6220 ± 40	6625–6293	6578–6368	–				
PPJ_FMA1_outer band	–	–	–	6547–6337	1.33–1.60	Vertical range of living microatolls	0.53	−0.48	1.64–2.24
PPJ_FMA2	Poz-83604	6320 ± 40	6736–6392	6668–6468	–				
PPJ_FMA2_RC3	Poz-106804	6280 ± 40	6691–6345	6656–6456	–				
PPJ_FMA2_RC4	Poz-106805	6340 ± 40	6758–6408	6643–6443	–				
PPJ_FMA2_outer band	–	–	–	6625–6425	0.81–1.14	Vertical range of living microatolls	0.53	−0.48	1.14–1.77
PPJ_FMA9	Poz-83614	6320 ± 40	6736–6392	6699–6517	–				
PPJ_FMA9_RC8	Poz-106810	6350 ± 40	6774–6421	6687–6505	–				
PPJ_FMA9_RC9	Poz-106811	6400 ± 40	6383–6476	6683–6501	–				
PPJ_FMA9_RC10	Poz-106812	6340 ± 35	6751–6411	6678–6496	–				
PPJ_FMA9_outer band	–	–	–	6665–6483	0.39–0.66	Vertical range of living microatolls	0.53	−0.48	0.70–0.130
Fossil corals									
PPJ_CB1	Poz-83617	6350 ± 40	6774–6421	–	0.10–0.35	Below LAT	–	–	–
PPJ_CB2	Poz-83618	6330 ± 40	6744–6398	–	0.10–0.59	Below LAT	–	–	–
PPJ_CB3	Poz-83619	6380 ± 35	6800–6452	–	0.14–0.59	Below LAT	–	–	–
PPJ_CB4	Poz-83620	6280 ± 35	6685–6348	–	−0.08–0.36	Below LAT	–	–	–

Note: The indicative meaning is based on the vertical difference between lowest astronomical tide (LAT) and mean high water neaps (MHWN) extracted from the OSU Tidal Prediction Software (Egbert and Erofeeva, 2002). For further details, see Supplemental Material Table S1 (text footnote 1). MSL—mean sea level.
*International Geo Sample Number (IGSN) is from Mann et al. (2019).
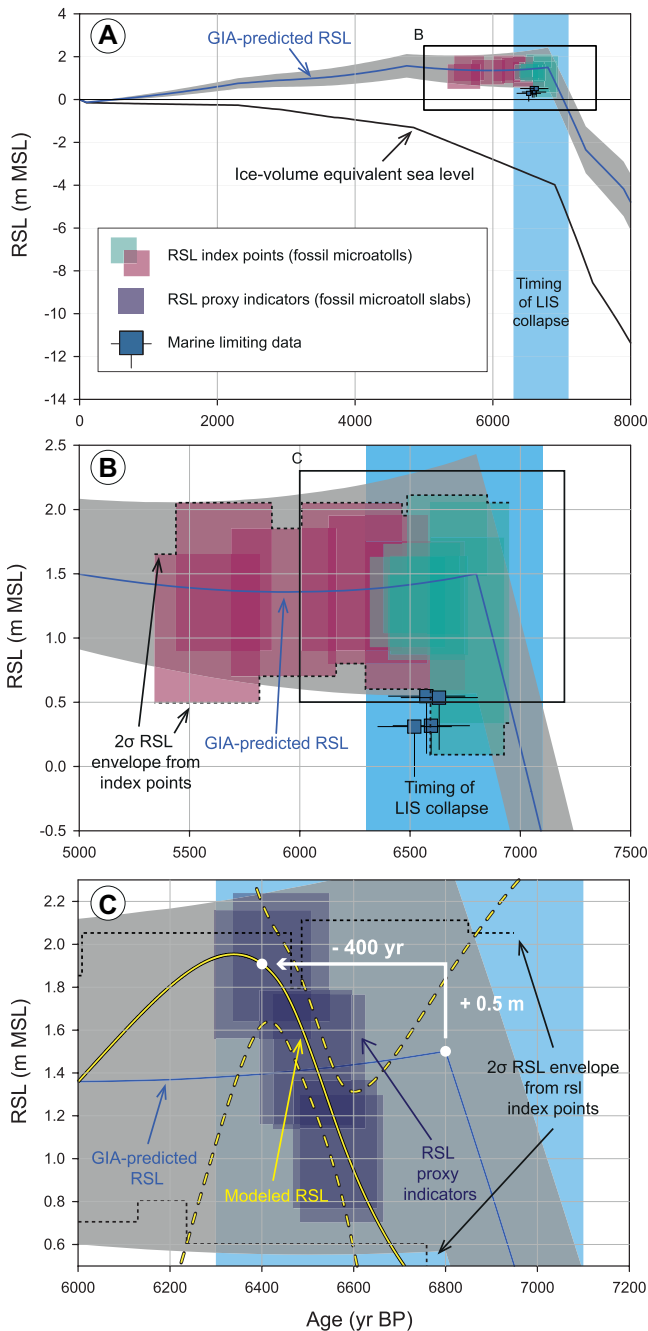†Possibly affected by ponding during growth according to transect profile T4.

Figure 3. Predicted, reconstructed, and modeled relative sea-level (RSL) trends and timing of final Laurentide ice sheet (LIS) melting (blue bar) based on Ullman et al. (2016). (A) RSL envelope based on index points and marine-limiting data compared to ice-volume equivalent sea level and RSL predicted based on geophysical modeling for that region (GIA—glacial isostatic adjustment; gray area indicates confidence limits; MSL—mean sea level). (B) Detailed comparison of RSL data and isostatic modeling shows that predicted RSL lies well within 2σ boundaries of reconstructed RSL. Marine-limiting data plot realistically below both predictions and reconstruction. (C) Microatoll slab data reveal rise of RSL within confidence limits of index points and isostatic model. Modeled RSL (yellow-black line) based on age-elevation information of microatoll growth increments indicates sustained RSL rise of ~1.3 m between 6.7 and 6.4 ka (solid line—median probability; long dashed lines—5th/95th percentiles).

MODELING GLACIAL ISOSTATIC ADJUSTMENT

The occurrence of microatoll RSL index points above coral marine-limiting data suggests a consistent reconstruction presented in this work (Fig. 3). Agreement between the RSL index points and the ANU glacial rebound solution has important implications regarding the potential of predictive isostatic models as tools with which to constrain future RSL variability. First, it is critical to acknowledge the site-specific geological environment that controls the regional isostatic response. Contrary to oceanic islands, for example, at far-field continental margins such as the present study area, the water load is not distributed symmetrically around the site. Accordingly, the isostatic response is a mixture of the mantle response to the distant ice unloading and the ocean response to the water load (Lambeck et al., 2014). Furthermore, the good fit between geological proxies and predictions shows that relatively simple, three-layer mantle solutions as solid-earth model components provide a predictive capability that is consistent with the accuracies of most RSL observations in southeast Asia (Mann et al., 2019).

CHRONOLOGY OF LIS MELTING

Proxy indicator data provide a Holocene RSL record on time scales <200 yr that is instructive for resolving ice dynamics. Hierarchical, statistical modeling of the data suggests a sustained RSL rise by ~1.3 m between 6.7 and 6.4 ka, which falls within the 2σ RSL envelope obtained from the individual microatolls that provided time-averaged information. The coherence between the two independent reconstructions and the nearly identical rates of modeled and predicted late-deglacial RSL rise indicate that the most likely explanation for the rapid rise is the final meltwater input from the LIS. Of note, the modeled RSL rise here culminated at 6.4 ± 0.1 ka and thus postdates assumed LIS deglaciation in the applied ice model by 400 yr. While a calibration of this ice model is straightforward due to underlying temporal resolution (500 yr bins), the reconstructed timing of LIS disappearance is significantly younger than that in the ice models proposed by Peltier (2004) and Peltier et al. (2015).

Currently, the most precise chronostratigraphic constraints place ultimate LIS melting between 7.1 and 6.3 ka (Carlson et al., 2008; Ullman et al., 2016). Our interpretation is consistent with these constraints, yet with improved temporal precision, and we suggest that the difference compared to Peltier's deglaciation chronology is a result of the underlying minimum-limiting radiocarbon data in their ice models.

Interestingly, the peak RSL highstand at 6.4 ± 0.1 ka is ~0.5 m above the predicted median highstand at the end of significant Northern Hemisphere deglaciation (Fig. 3). However,

channel behind the rubble rampart and indicate that RSL first reached its present position before ca. 7 ka. Synthesized with recently standardized RSL data from nearby Teluk Awur (Azmy et al., 2010; Mann et al., 2019), the complete record suggests that RSL was ~1.3 ± 0.7 m above present between 6.9 and 5.3 ka (Fig. 3).

This is consistent with predicted RSL because RSL would have risen rapidly during the late deglacial period as a result of the increase in ocean volume. A subsequent change in the rate of ice-volume equivalent sea-level (ESL) rise, coinciding with a period of slowly falling predicted RSL, was caused by the assumed termination of LIS deglaciation at 6.8 ka by the model and reflects the relaxation of the mantle

below the ocean crust and the elastic lithosphere response. A period of ~2000 yr followed, during which the ESL contribution from Antarctica of ~2.5 m and loading of the ocean basin adjacent to the study site were nearly balanced.

Significantly, the temporally higher-resolution RSL proxy indicators from coral slabs revealed a RSL trend that would not have been captured if only the less precise fossil microatoll surfaces had been analyzed. Statistically modeled RSL based on age-elevation information from the youngest and oldest growth bands showed a significant and continuous rise by ~1.3 m between 6.7 and 6.4 ka, with maximum significant rates of 6.2 ± 5.0 mm/yr (2σ) between 6.54 and 6.53 ka (Figs. 2 and 3; Table S2).

as the reconstructed highstand lies within the confidence limits of the predictions, the difference may be resolved through another combination of Earth-model viscosity parameters. Alternatively, the difference could indicate a larger Antarctic contribution to ESL than is assumed in the ice model. Additional, accurate RSL data across the basin margins, from offshore islands and deeply indented bays and estuaries, are important for analyzing spatial differences between sites in Indonesia to further separate lower- and upper-mantle responses and provide corrective terms to the global ice-volume function (Nakada and Lambeck, 1988).

REFERENCES CITED
Ashe, E.L., Cahill, N., Hay, C., Khan, N.S., Kemp, A., Engelhart, S.E., Horton, B.P., Parnell, A.C., and Kopp, R.E., 2019, Statistical modeling of rates and trends in Holocene relative sea level: Quaternary Science Reviews, v. 204, p. 58–77, https://doi.org/10.1016/j.quascirev.2018.10.032.

Azmy, K., Edinger, E., Lundberg, J., and Diegor, W., 2010, Sea level and paleotemperature records from a mid-Holocene reef on the north coast of Java, Indonesia: International Journal of Earth Sciences, v. 99, no. 1, p. 231–244, https://doi.org/10.1007/s00531-008-0383-3.

Carlson, A.E., LeGrande, A.N., Oppo, D.W., Came, R.E., Schmidt, G.A., Anslow, F.S., Licciardi, J.M., and Obbink, E.A., 2008, Rapid early Holocene deglaciation of the Laurentide ice sheet: Nature Geoscience, v. 1, no. 9, p. 620–624, https://doi.org/10.1038/ngeo285.

Dyke, A., and Prest, V., 1987, Late Wisconsinan and Holocene history of the Laurentide ice sheet: Géographie Physique et Quaternaire, v. 41, no. 2, p. 237–263, https://doi.org/10.7202/032681ar.

Dyke, A., Andrews, J., Clark, P., England, J., Miller, G., Shaw, J., and Veillette, J., 2002, The Laurentide and Innuitian ice sheets during the Last Glacial Maximum: Quaternary Science Reviews, v. 21, no. 1–3, p. 9–31, https://doi.org/10.1016/S0277-3791(01)00095-6.

Egbert, G.D., and Erofeeva, S.Y., 2002, Efficient inverse modeling of barotropic ocean tides: Journal of Atmospheric and Oceanic Technology, v. 19, no. 2, p. 183–204, https://doi.org/10.1175/1520-0426(2002)019<0183:EIMOBO>2.0.CO;2.

Heaton, T.J., Köhler, P., Butzin, M., Bard, E., Reimer, R.W., Austin, W.E., Ramsey, C.B., Grootes, P.M., Hughen, K.A., and Kromer, B., 2020, Marine20—The marine radiocarbon age calibration curve (0–55,000 cal BP): Radiocarbon, v. 62, no. 4, p. 779–820, https://doi.org/10.1017/RDC.2020.68.

Kench, P.S., McLean, R.F., Owen, S.D., Ryan, E., Morgan, K.M., Ke, L., Wang, X., and Roy, K., 2020, Climate-forced sea-level lowstands in the Indian Ocean during the last two millennia: Nature Geoscience, v. 13, no. 1, p. 61–64, https://doi.org/10.1038/s41561-019-0503-7.

Khan, N.S., Horton, B.P., Engelhart, S., Rovere, A., Vacchi, M., Ashe, E.L., Törnqvist, T.E., Dutton, A., Hijma, M.P., and Shennan, I., 2019, Inception of a global atlas of sea levels since the Last Glacial Maximum: Quaternary Science Reviews, v. 220, p. 359–371, https://doi.org/10.1016/j.quascirev.2019.07.016.

Lambeck, K., 1993, Glacial rebound and sea-level change: An example of a relationship between mantle and surface processes: Tectonophysics, v. 223, no. 1–2, p. 15–37, https://doi.org/10.1016/0040-1951(93)90155-D.

Lambeck, K., and Chappell, J., 2001, Sea level change through the last glacial cycle: Science, v. 292, no. 5517, p. 679–686, https://doi.org/10.1126/science.1059549.

Lambeck, K., Rouby, H., Purcell, A., Sun, Y., and Sambridge, M., 2014, Sea level and global ice volumes from the Last Glacial Maximum to the Holocene: Proceedings of the National Academy of Sciences of the United States of America, v. 111, no. 43, p. 15,296–15,303, https://doi.org/10.1073/pnas.1411762111.

Lambeck, K., Purcell, A., and Zhao, S., 2017, The North American late Wisconsin ice sheet and mantle viscosity from glacial rebound analyses: Quaternary Science Reviews, v. 158, p. 172–210, https://doi.org/10.1016/j.quascirev.2016.11.033.

Mann, T., Bender, M., Lorscheid, T., Stocchi, P., Vacchi, M., Switzer, A.D., and Rovere, A., 2019, Holocene sea levels in southeast Asia, Maldives, India and Sri Lanka: The SEAMIS database: Quaternary Science Reviews, v. 219, p. 112–125, https://doi.org/10.1016/j.quascirev.2019.07.007.

Meltzner, A.J., and Woodroffe, C.D., 2015, Coral microatolls, in Shennan, I., et al., Handbook of Sea-Level Research: New York, John Wiley & Sons, p. 125–145.

Mitrovica, J., and Milne, G., 2002, On the origin of late Holocene sea-level highstands within equatorial ocean basins: Quaternary Science Reviews, v. 21, no. 20–22, p. 2179–2190, https://doi.org/10.1016/S0277-3791(02)00080-X.

Mitrovica, J.X., and Peltier, W.R., 1991, On postglacial geoid subsidence over the equatorial oceans: Journal of Geophysical Research: Solid Earth, v. 96, no. B12, p. 20,053–20,071, https://doi.org/10.1029/91JB01284.

Nakada, M., and Lambeck, K., 1988, The melting history of the late Pleistocene Antarctic ice sheet: Nature, v. 333, no. 6168, p. 36–40, https://doi.org/10.1038/333036a0.

Peltier, W.R., 2004, Global glacial isostasy and the surface of the ice-age Earth: The ICE-5G (VM2) model and GRACE: Annual Review of Earth and Planetary Sciences, v. 32, p. 111–149, https://doi.org/10.1146/annurev.earth.32.082503.144359.

Peltier, W.R., Argus, D., and Drummond, R., 2015, Space geodesy constrains ice age terminal deglaciation: The global ICE-6G_C (VM5a) model: Journal of Geophysical Research: Solid Earth, v. 120, no. 1, p. 450–487, https://doi.org/10.1002/2014JB011176.

Ramsey, C.B., 2008, Deposition models for chronological records: Quaternary Science Reviews, v. 27, no. 1–2, p. 42–60, https://doi.org/10.1016/j.quascirev.2007.01.019.

Scoffin, T.P., and Stoddart, D., 1978, The nature and significance of microatolls: Philosophical Transactions of the Royal Society of London B–Biological Sciences, v. 284, no. 999, p. 99–122.

Shennan, I., Long, A.J., and Horton, B.P., eds, 2015, Handbook of Sea-Level Research: New York, John Wiley & Sons, 600 p., https://doi.org/10.1002/9781118452547.

Simons, W., Socquet, A., Vigny, C., Ambrosius, B., Haji Abu, S., Promthong, C., Subarya, C., Sarsito, D., Matheussen, S., and Morgan, P., 2007, A decade of GPS in Southeast Asia: Resolving Sundaland motion and boundaries: Journal of Geophysical Research: Solid Earth, v. 112, no. B6, B06420, https://doi.org/10.1029/2005JB003868.

Smithers, S.G., and Woodroffe, C.D., 2000, Microatolls as sea-level indicators on a mid-ocean atoll: Marine Geology, v. 168, no. 1–4, p. 61–78, https://doi.org/10.1016/S0025-3227(00)00043-8.

Sobolev, S.V., Babeyko, A.Y., Wang, R., Hoechner, A., Galas, R., Rothacher, M., Sein, D.V., Schröter, J., Lauterjung, J., and Subarya, C., 2007, Tsunami early warning using GPS-shield arrays: Journal of Geophysical Research: Solid Earth, v. 112, no. B8, B08415, https://doi.org/10.1029/2006JB004640.

Southon, J., Kashgarian, M., Fontugne, M., Metivier, B., and Yim, W.W., 2002, Marine reservoir corrections for the Indian Ocean and Southeast Asia: Radiocarbon, v. 44, no. 1, p. 167–180, https://doi.org/10.1017/S0033822200064778.

Ullman, D.J., Carlson, A.E., Hostetler, S.W., Clark, P.U., Cuzzone, J., Milne, G.A., Winsor, K., and Caffee, M., 2016, Final Laurentide ice-sheet deglaciation and Holocene climate–sea level change: Quaternary Science Reviews, v. 152, p. 49–59, https://doi.org/10.1016/j.quascirev.2016.09.014.

Woodroffe, C.D., McGregor, H.V., Lambeck, K., Smithers, S.G., and Fink, D., 2012, Mid-Pacific microatolls record sea-level stability over the past 5000 yr: Geology, v. 40, no. 10, p. 951–954, https://doi.org/10.1130/G33344.1.

Yokoyama, Y., and Esat, T.M., 2015, Coral reefs, in Shennan, I., et al., Handbook of Sea-Level Research: New York, John Wiley & Sons, p. 104–124.

Printed in USA